ACS ES&T Engineering

pubs.acs.org/estengg

Article

Degradation of Microplastics by a Thermal Fenton Reaction

Kunsheng Hu, Peng Zhou, Yangyang Yang, Tony Hall, Gang Nie, Yu Yao, Xiaoguang Duan,* and Shaobin Wang*

Cite This: *ACS EST Engg.* 2022, 2, 110–120

Read Online

ACCESS | Metrics & More | Article Recommendations | Supporting Information

ABSTRACT: Microplastics (MPs) are ubiquitous in the environment and are infiltrating the food chain, causing potential risks to living beings. However, current methods of MP removal from an aqueous environment are limited by low efficiency. Advanced oxidation processes (AOPs) are emerging techniques for MP purification. Herein, a hydrothermal coupled Fenton system is developed for decomposition of ultrahigh-molecular-weight polyethylene, achieving 95.9% weight loss in 16 h and 75.6% mineralization efficiency in 12 h. The high effectiveness is attributed to the synergy of hydrothermal hydrolysis, proton-rich environment, and massive production of hydroxyl radicals. The system is also efficient to remediate different petroleum-based plastics and maintains high efficiency in practical water bodies. Characterizations revealed a two-stage degradation process: chain unfolding/stretching and oxidation, giving rise to the formation of carbonyl groups and decreased crystallinity of MPs during the hydrothermal treatment. The chain stretching stage is pivotal to the whole treatment because it remarkably facilitates subsequent chain cleavage and Fenton oxidation. This study provides a new approach to removing MPs in water bodies and new insights into MP degradation by the AOP technology.

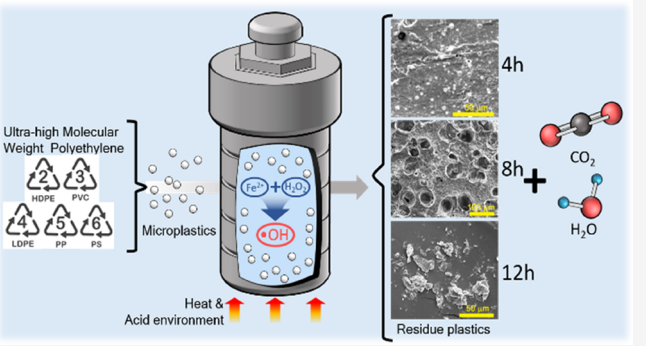

KEYWORDS: *microplastics, hydrothermal treatment, Fenton reaction, two-stage degradation, advanced oxidation technology*

INTRODUCTION

Since plastics' industrialization in 1950s, the global production of plastics soared and reached 368 million tonnes in 2019.[1] A recent research estimated that 1.1 billion tonnes of plastics will be produced in 2050.[2] Particularly, plastics with sizes <5 mm are termed as microplastics (MPs).[3] MPs come either directly from industrial production as primary sources for specific purposes (e.g., facial cleansers and polishing agents)[4] or indirectly from fragmentation of larger pieces of plastics as secondary sources through UV irradiation or abrasion (e.g., polypropylene (PP) and polyethylene (PE) fibers from fishery nets).[5] In recent years, different types of MPs have been detected in freshwater systems,[6] oceans,[7] terrestrial soil,[8] air,[9] and even in Arctic[10] and Antarctic areas.[11] Worse still, MPs extensively exist in daily-life products, such as cosmetics,[4] tea bags,[12] table salts,[9] tap water,[13] bottled water,[14] and milk.[15] Nevertheless, the majority of mismanaged plastic wastes is transported via sewage, rivers, and eventually to the oceans.[16] Thus, MPs in sewage and wastewater have become a potential hazard in future water and food supply.

The characteristics of abundance and small size make MPs more likely to be ingested by marine life. Until now, MPs have been found in 92% of at least 690 marine species that encountered marine debris.[17] MPs can cause physical impacts on wildlife via internal or external abrasion and digestive tract blockage.[18] In addition, pollutants adsorbed on MPs and hazardous additives contained in MPs render MPs to act as a vector to gather and transfer toxic pollutants, causing potential threats to wildlife.[19,20] More than half of priority pollutants given out by the U.S. Environmental Protection Agency and European Union are related to plastic debris.[19] In addition, MPs have already been found in human lung tissue and stool.[21,22] Therefore, removing MPs from the environment is stringent, considering their distribution, negative biological impacts, and soaring production.

In the last decade, many techniques have been devised to degrade MPs. Recently, these strategies and technologies have been comprehensively reviewed and discussed.[23] Technologies such as cogasification,[24] thermal pyrolysis,[25] and microwave-initiated catalytic reactions[26] have been proved effective to remove MPs. However, these techniques were based on solid-state reactions. MPs in water are featured with small sizes and ultralarge quantities. Nevertheless, wastewater treatment plants can achieve a MP retention rate of 98.3% via a conventional

Received: September 5, 2021
Revised: November 3, 2021
Accepted: November 12, 2021
Published: November 24, 2021

activated sludge process and a pilot-scale membrane bioreactor; there are approximately 1×10^7 MPs discharged daily in the final effluent.[27] MP removal by adsorption or filtration is an effective way to relieve MP contamination, but MPs still exist in the adsorbents/membrane and require further treatments. Micromotors were also designed to remove MPs via generating adsorptive bubbles,[28] but the efficiency needs to be further improved. Recently, advanced oxidation processes (AOPs) have been applied in MP degradation in the aqueous environment, utilizing diverse reactive oxygen species (ROS).[29,30] We innovatively coupled hydrothermal conditions with persulfate-based AOPs to intensify the oxidation and mineralization efficiency.[29] It was shown that sulfate radicals ($SO_4^{\bullet-}$, E^0 = 3.1 V vs normal hydrogen electrode [NHE]) have great capacity of degrading cosmetic polyethylene MPs. On the other hand, Fenton's reagent (Fe^{2+}/H_2O_2) can generate hydroxyl radicals ($^{\bullet}OH$, E^0 = 2.7 V vs NHE) to degrade persistent organic pollutants with advantages of high performance, simplicity, and nontoxicity.[31] In this study, we first applied the intensified Fenton system to directly purify MPs in water. In previous MP treatment, Fenton's reagent was usually applied as a fast and efficient method to isolate MPs from wastewater[32] and organic-rich matrices[33] by digesting organic compounds through oxidation. This process will not significantly impact the properties of MPs at room temperature. The U.S. National Oceanic and Atmospheric Administration (NOAA) also recommended to use Fenton's reagent to extract MPs from various environments.[34] A recent study showed that Fenton's reagent accelerated surface aging of MPs at room temperature, despite that the oxidation rate was low.[35]

In this study, we first coupled the Fenton reaction with a hydrothermal process for direct decomposition of refractory MP polymers in water. We analyzed the chemical, structural, and morphological changes of MPs before and after the treatment by multiple characterizations and analytical techniques. We found that both hydrothermal conditions and Fenton oxidation played indispensable roles in MP removal. MPs experienced significant changes in carbon chain scission and formation of carbonyl groups. The performances of the integrated system toward different types of MPs were evaluated. Experiments on real-life plastics and in real water matrices were also performed. In addition, the toxicity of degradation intermediates was evaluated using *Escherichia coli* (*E. coli*) as a probe.[36,37] The outcomes of this study will provide basis and inspiration for future research on optimization of Fenton or Fenton-like systems toward MP purification.

EXPERIMENTAL SECTION

Pretreatment and Preparation of Microplastics. For removal of the acid and hydroxy groups on the ultrahigh-molecular-weight polyethylene (UHMWPE) MPs, a pretreatment is required. To be specific, 2.5 g of MPs was added into 50 mL of 2 M aqueous NaOH and stirred at 500 rpm at 40 °C for 24 h, followed by vacuum filtration, and then washed with ultrapure water until pH of the filtrate reached neutral. The obtained MPs were dried in air for 3 days before use. Polystyrene (PS) MPs were obtained by ball-milling PS pellets with a planetary mill (FRITSCH PULVERISETTE 7 with zirconia balls and vials) at a low speed of 300 rpm overnight. It was set to operate for 2 min every 7 min to prevent high-temperature damage to MPs. The pellets of poly(ethylene terephthalate) (PET), high-density polyethylene (HDPE), low-density polyethylene (LDPE), and PP were smashed by a grinder (IKA A 11 basic analytical mill) with 10 s operation in every 10 min. All of the obtained particles were filtered by a 100 μm stainless steel sieve followed by washing with ethanol and water several times. The MPs were then air-dried at room temperature for 3 days before use. The ball milling is capable to produce finer MPs than the grinder. The MPs from a facial cleanser were extracted by washing with ultrapure water several times under magnetic stirring at 500 rpm for 24 h. The MPs were filtered with 0.45 μm cellulose acetate (CA) membranes, washed several times, and then air-dried for 3 days. The MPs from plastic bags (LDPE), plastic wraps (LDPE), and milk bottles (HDPE) were made by cutting the products with scissors into debris smaller than 5 mm.

Fenton Oxidation Procedure. The oxidation was performed in a 200 mL Teflon autoclave at 140 °C in an oven. Overall, 1 g L^{-1} certain types of MPs (UHMWPE, LDPE, HDPE, PS, poly(vinyl chloride) (PVC), PP, or PET) were first dispersed in 150 mL of ultrapure water by magnetic stirring vigorously at 1500 rpm for 10 min. To prevent the generation of iron sludge and facilitate the measurement of weight loss and characterization of MPs, the solution pH was adjusted to the acidic condition ($c(H^+)$ = 0.2 M) using hydrochloric acid or sulfuric acid unless specifically mentioned. $FeSO_4{\cdot}7H_2O$ (4 mM) was dissolved in the solution, and 200 mM H_2O_2 was then added into the autoclave to trigger the reaction (room temperature), followed by sealing and transferring the autoclave rapidly in a preheated oven. After the reaction, the autoclave was cooled slowly to room temperature in the oven. Then, MPs were collected by vacuum filtration with a preweighed 0.45 μm CA membrane. To prevent the corrosion of the membrane, the solution was diluted 10 times in advance. If the iron sludge was produced, the filter residues were washed with hydrochloric acid (37%) by stirring at 500 rpm for 24 h, and then diluted and filtered to obtain the solid product. The product was dried in air for 3 days before weighing. The Fenton experiment was carried out in duplicates and the mean values are presented. Quenching experiments were performed with different concentrations of methanol (0−500 mM). Blank and comparative experiments (Fenton reagents free and lower temperatures) were carried out accordingly. The oxidation efficiency was evaluated with the following equation (eq 1)

$$\text{weight loss (\%)} = \frac{W_t - W_0}{W_0} \times 100\% \quad (1)$$

where W_t is the weight of remaining MPs after the Fenton reaction and W_0 is the initial weight of MPs.

MP Characterizations. The morphology changes of MPs were investigated by scanning electron microscopy (SEM, FEI Quanta 450). X-ray diffraction (XRD) was carried out using a Rigaku MiniFlex 600 X-ray diffractometer. The functional groups and the molecular structures of MPs were examined by Fourier transform infrared (FTIR) spectroscopy (Nicolet 6700 Thermofisher) and Raman spectroscopy (HORIBA LabRAM HR Evolution) equipped with a green laser at 532 nm. The chemical states of carbon and oxygen were obtained from X-ray photoelectron spectroscopy (XPS) with Mg Kα X-ray. The size distributions of MPs were recorded by a Mastersizer 2000-Malvern using ethanol as a solvent. Differential scanning calorimetry was carried out by thermogravimetric analysis-differential scanning calorimeter (TGA−DSC, Mettler Tole-

https://doi.org/10.1021/acsestengg.1c00323
ACS EST Engg. 2022, 2, 110−120

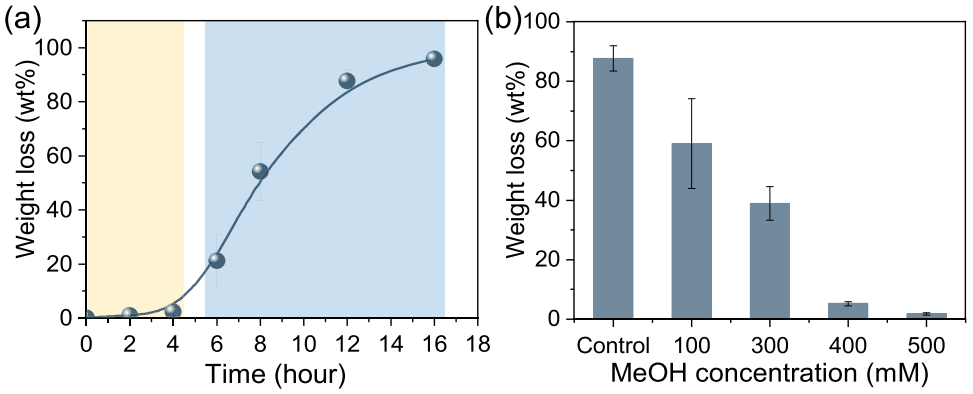

Figure 1. (a) MP degradation performance of the Fenton system and (b) quenching experiments with different amounts of methanol (experimental conditions: Fe^{2+}: 4 mM, H_2O_2: 200 mM, UHMWPE MPs: 1 g L^{-1}, temperature: 140 °C).

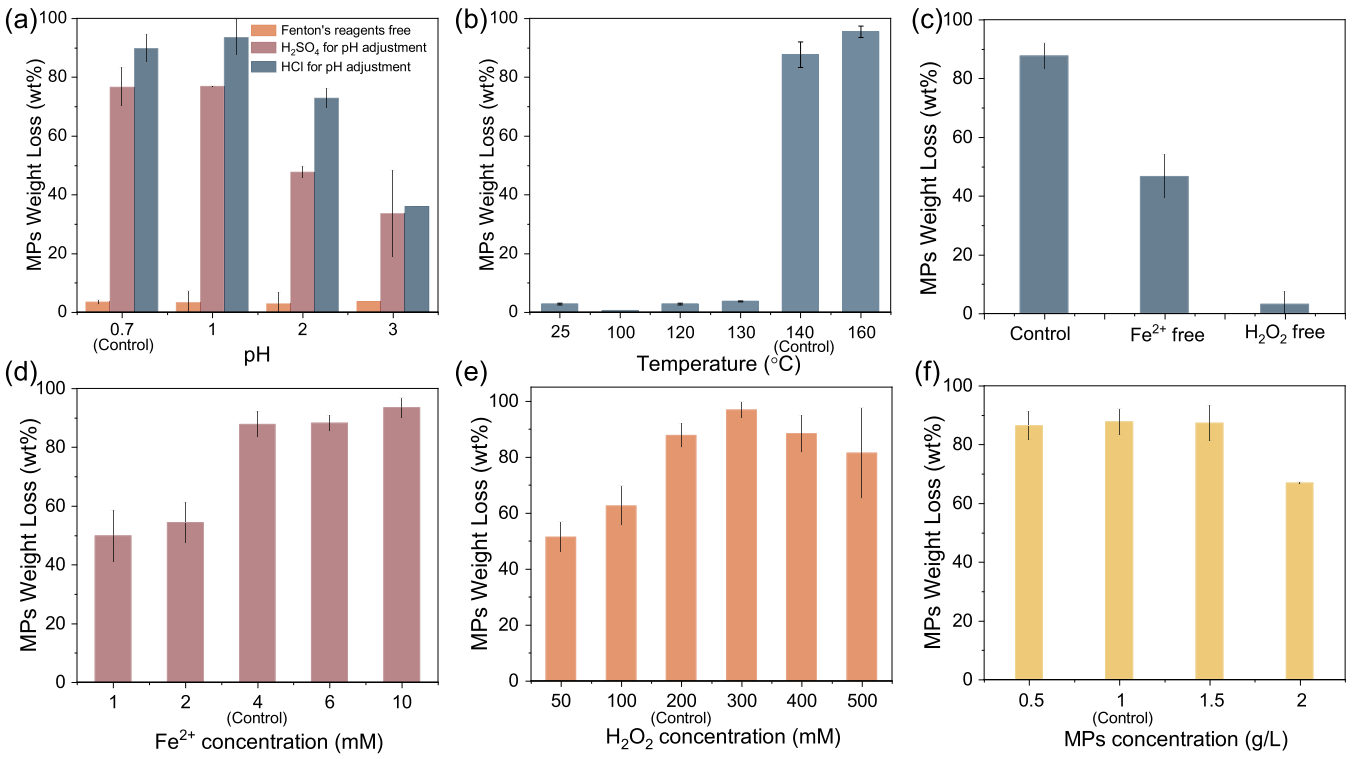

Figure 2. Weight loss of MPs under different conditions: (a) pH value, (b) temperature, (c) Fe^{2+} free or H_2O_2 free, (d) Fe^{2+} concentration, (e) H_2O_2 dosage, and (f) MP loading (control conditions: Fe^{2+}: 4 mM; H_2O_2: 200 mM; UHMWPE MPs: 1 g L^{-1}; hydrothermal temperature: 140 °C; time: 12 h).

do). MPs (2−4 mg) were placed in an aluminum pan with 50 mL min^{-1} N_2. The initial heating rate was 10 °C min^{-1} before 120 °C, followed by 5 °C min^{-1} between 120 and 180 °C. The subsequent cooling rate was the same as the heating period.

Toxicity Evaluation. The toxicity of the filtrates was evaluated with a modified filter paper disk method.[36,37] Solutions for the toxicity evaluation were prepared by pH adjustment to 7.5−8.0 and filtration. The bacterial strain of *E. coli* was thawed from a stock (−80 °C) and cultivated in the Luria−Bertani (LB) Lennox medium with 50 μg mL^{-1} streptomycin at 37 °C overnight. Then, 0.5 mL of obtained *E. coli* was mixed with 9.5 mL of LB Lennox media (containing 50 μg mL^{-1} streptomycin), and cultivated at 37 °C for 80 min to reach its exponential phase (optical density at 600 nm was around 0.6). Subsequently, the solution was diluted 300 times with the LB Lennox medium. About 0.1 mL of the inoculum was added to an agar plate (containing 50 μg mL^{-1} streptomycin) and spread evenly over the surface. Afterward, filter papers that were rinsed in filtrates for 24 h were placed gently on the agar surface, which was then cultivated at 37 °C overnight. The size of the inhibition zone represents the toxicity of the tested solution. Blank filter papers rinsed in ultrapure water and 1 mg mL^{-1} ampicillin were regarded as positive and negative control tests, respectively. The chemicals used and quality control are described in Text S1 of the Supporting Information (SI).

RESULTS AND DISCUSSION

MP Degradation Performance. Figure 1a shows MP removal by the hydrothermal Fenton system. In the first 4 h, the weight of MPs did not change much. However, rapid degradation occurred in 4−16 h, achieving 95.9% weight loss

https://doi.org/10.1021/acsestengg.1c00323
ACS EST Engg. 2022, 2, 110−120

of MPs. The total organic carbon (TOC) value after the 12 h reaction reached 104.0 mg L^{-1}, and the corresponding mineralization rate was 75.6% (see Text S2 and Table S1). Figure S1 shows that MP degradation follows the pseudo-first-order kinetic model for the two stages. The reaction rate constants in the first (0−4 h) and second stages (6−16 h) were 0.0058 ± 0.0006 and 0.299 ± 0.009 h^{-1}, respectively. We suppose that the initial stage (0−4 h) did not directly cause weight loss but significantly changed the structure/chemistry of MPs via breaking and unfolding the condensed molecule chains,[29] which is beneficial for the subsequent radical oxidation in the second stage to decompose the segments.

To figure out the responsible ROS for the MP loss, radical quenching experiments were performed using methanol as an oxidation terminator due to its fast reaction rate with •OH radicals (Figure 1b). The addition of methanol showed distinct retardation to the weight loss of MPs, and the increase of methanol loading caused further inhibition of oxidation. When the methanol dosage reached 500 mM, only 1.77% MP loss was attained. The radical quenching tests prove that •OH is the primary ROS accounting for MP decomposition.

The impacts of reaction parameters on MP removal were evaluated under different conditions. As shown in Figure 2a, the Fenton system was effective at a H^+ concentration between 0.2 and 1 × 10^{-3} M (pH = 0.7−3), and the removal efficiency decreased gradually as pH increased. Higher pH might lead to the direct hydrolysis of H_2O_2 and severe precipitation of Fe^{3+} into amorphous ferric oxyhydroxides, which are considerably less Fenton reactive, dramatically reducing the oxidative capacity of the system.[31,38−40] At 140 °C, the ionization product constant of water is 11.7,[41] which means the concentration of hydroxyl ions ($c(OH^-)$) roughly increased by $10^{2.3}$ times (assuming $c(H^+)$ is constant) compared to room temperature. Thus, the values of $c(OH^-)$ at initial pH = 0.7, 1, 2, and 3 at 140 °C equal to those at pH = 3, 3.3, 4.3, 5.3, respectively, at 25 °C. A higher concentration of OH^- would facilitate the decomposition of H_2O_2 into H_2O and O_2 (eq S1),[42] restraining ROS generation and eventually reducing MP oxidation capacity. In contrast, a higher concentration of H^+ will drive MP oxidation to form hydroperoxide $(-CH_2-HCOOH-CH_2-)_n$, which then splits into new free oxy radicals $(-CH_2-HCO^•-CH_2-)_n$ and •OH, respectively (eqs S2 and S3).[43] Hydroxyl radicals, in turn, attack MPs and promote degradation. However, at a pH value lower than 1, the MP decomposition rate slightly decreased. This might be due to the fact that an ultrahigh concentration of H^+ might further quench •OH to form H_2O (eq S4), consuming ROS and decreasing the oxidation capacity of the Fenton system.[31,38] Therefore, under hydrothermal conditions, the optimal initial pH value of the thermal Fenton system should be more acidic than the ambient environment (pH of 2−4).

The high-concentration protons (0.2 M $c(H^+)$) may partially destroy polymer structures, but they are not the main driving force for the significant degradation in the Fenton system. Moreover, the thermal Fenton system showed a better efficiency using hydrochloric acid to adjust the acidity than that using sulfuric acid. This implied that the presence of Cl^- accelerated the degradation of MPs. The chlorine ions would react with H_2O_2 and •OH to produce chlorine radicals ($Cl^•$, E^0 = 2.41 V vs NHE and $Cl_2^{•-}$, E^0 = 2.09 V vs NHE[44]), which are also oxidative and would contribute to MPs degradation. Overall, H^+ will facilitate Fenton-based MP degradation in two possible aspects: (1) preventing hydrolysis of H_2O_2 and precipitation of Fe^{3+} and (2) promoting the formation of hydroperoxide $(-CH_2-HCOOH-CH_2-)_n$ to favor oxidative hydrolysis of plastics.

Figure 2b shows the effect of hydrothermal temperature on MP weight loss. When the temperature is lower than 140 °C, there was almost no weight loss. However, once the hydrothermal temperature was elevated to 140 °C, the decomposition efficiency remarkably increased to almost 90%, and 95.5% removal at 160 °C. Interestingly, the melting point of UHMWPE (Sigma-Aldrich) is 144 °C. This suggests that the effective oxidation did not initiate until the temperature reached a certain point close to but not necessarily reaching the melting point of the polymer. We suppose that, when the environment temperature was lower than that temperature, the densely compact polymer chains and low surface area of MPs hindered ROS attack and oxidation, resulting in a low removal rate. Once the reaction reached a certain temperature, the carbon chain started to stretch and open, which increased the surface area of MPs. In addition, the higher temperature would facilitate radical generation both thermodynamically and kinetically.[31] The bare Fenton system and bare 140 °C experiments (Figure 2a,b) also evidence that the synergistic effect of heat and Fe^{2+} activation remarkably enhanced the radical generation efficiency. Therefore, a favorable high temperature is pivotal in MP degradation because it not only unfolds the densely packed macromolecules but also accelerates radical production, thereby significantly intensifying the decomposition process.

The influences of Fe^{2+} and H_2O_2 dosages on the thermal Fenton system were investigated. In Figure 2c, over 40% MPs were removed without Fe^{2+}. However, if Fe^{2+} was added without H_2O_2, MPs barely decomposed. Thus, H_2O_2 was indispensable in the thermal Fenton system, and the presence of Fe^{2+} further boosted H_2O_2 activation and •OH generation. When Fe^{2+} concentration increased from 1 to 4 mM, more MPs were degraded (Figure 2d). When the dosage of Fe^{2+} was above 4 mM (4−10 mM), the degradation rate only improved slightly. The overdosed Fe^{2+} might further scavenge •OH due to its reductive nature. Although *in situ* quantification of Fe^{2+} and Fe^{3+} will help reveal the mechanism, such an evaluation is hardly performed under hydrothermal conditions. In terms of H_2O_2 dosage, MP weight loss increased along with the increased level of H_2O_2 from 50 to 300 mM (Figure 2e). However, the efficiency dropped when the excess amounts of H_2O_2 (400−500 mM) were introduced. Overdosed H_2O_2 will compete with MPs to react with •OH via eq S5.[31,38] Therefore, the optimal dosages of Fe^{2+} and H_2O_2 are 4 and 300 mM, respectively. Figure 2f shows the MP removal capacity of the thermal Fenton system. When the system contained 0.5−1.5 g L^{-1} MPs, the degradation efficiency stabled at ca. 87%. When the MP dosage was increased to 2 g L^{-1}, the weight loss dropped to 66.9%. Insufficient Fe^{2+} and H_2O_2 should account for the lower efficiency at a high MP concentration due to the lack of •OH.[38]

We compared the thermal Fenton system with other typical homogeneous systems in Figure S2. Compared with $SO_4^{•-}$-based systems using peroxymonosulphate (PMS) or persulphate (PDS) as the parent peroxides activated by base or metals, the Fenton reaction exhibited a higher efficiency in MP degradation. Apart from UHMWPE, the thermal Fenton system was also used to degrade other types of microscopic plastic polymers (e.g., PP, PET, HDPE, PVC, LDPE, and PS), as shown in Figure 3a. The acidic environment has no

https://doi.org/10.1021/acsestengg.1c00323
ACS EST Engg. 2022, 2, 110−120

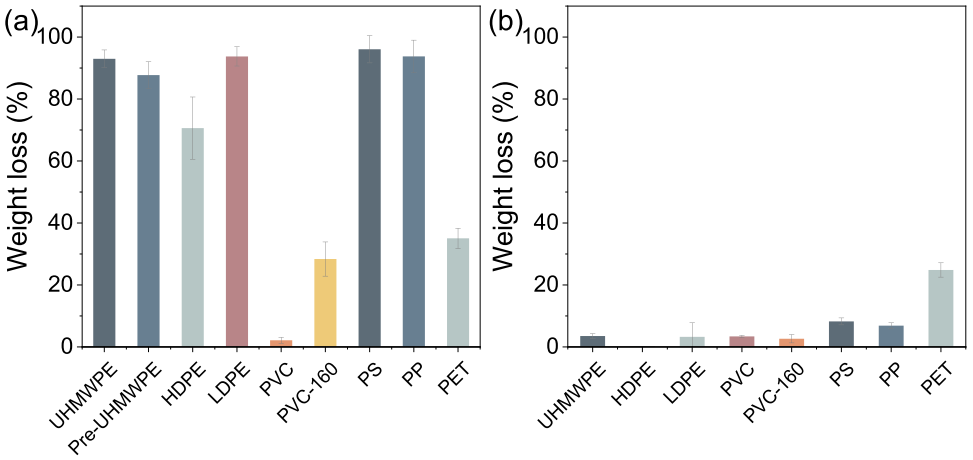

Figure 3. Weight loss of different types of microplastics (a) after thermal-assisted Fenton treatment and (b) thermal treatment with 0.2 M H^+ (experimental conditions: Fe^{2+}: 4 mM, H_2O_2: 200 mM, MPs: 1 g L^{-1}, temperature: 140 °C).

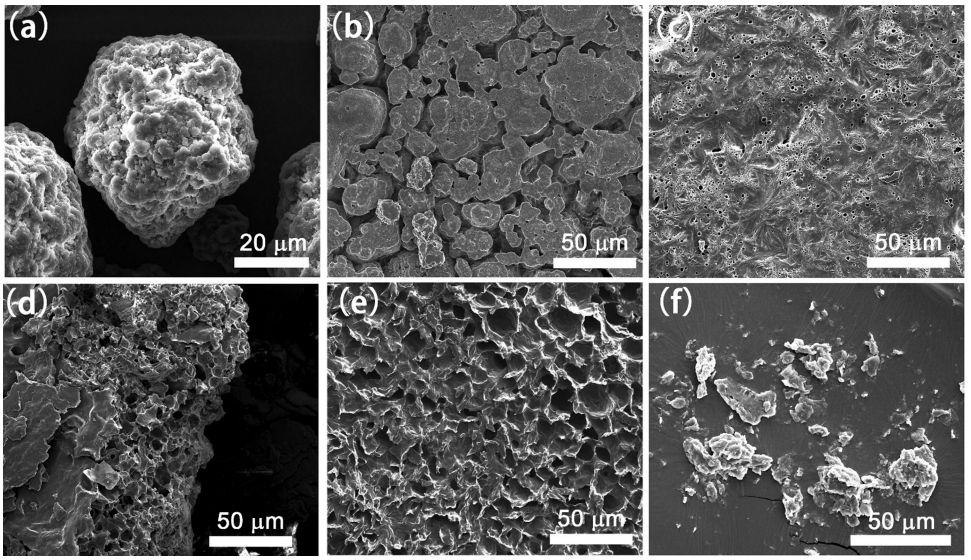

Figure 4. SEM images of MPs experienced different durations of Fenton oxidation: (a) 0 h, (b) 2 h, (c) 4 h, (d) 6 h, (e) 8 h, and (f) 12 h (Fe^{2+}: 4 mM, H_2O_2: 200 mM, UHMWPE MPs: 1 g L^{-1}, temperature: 140 °C).

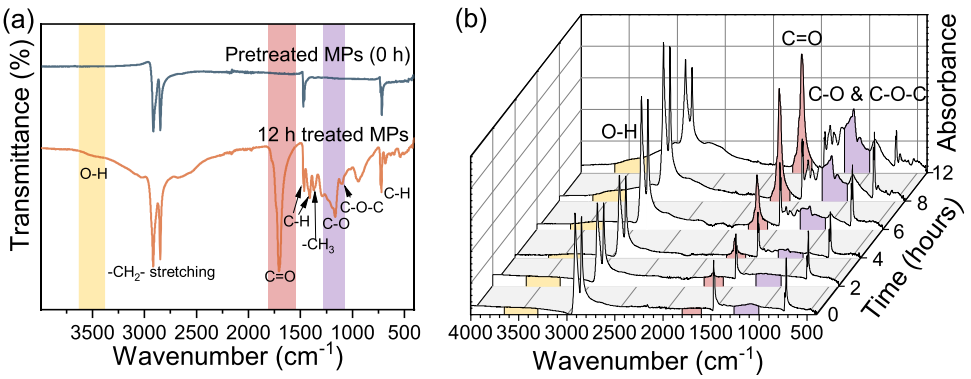

Figure 5. FTIR spectra of MPs experienced different durations of Fenton treatment: (a) transmittance spectra of pretreated and 12 h-treated MPs and (b) absorbance spectra of MPs after 0−12 h treatments (experimental conditions: Fe^{2+}: 4 mM, H_2O_2: 200 mM, UHMWPE MPs: 1 g L^{-1}, temperature: 140 °C).

hydrolysis effect on most of the plastics (HDPE, PVC, LDPE, PP, and PS) under hydrothermal conditions (Figure 3b). As for HDPE, LDPE, PS, and PP, 90% weight loss was attained after the reaction. The lower degradation rate of HDPE than that of LDPE may be attributed to the higher density and fewer branches of HDPE, which require a longer activation time for chain stretching and opening. Almost no oxidation appeared for PVC at 140 °C, but the weight loss reached

https://doi.org/10.1021/acsestengg.1c00323
ACS EST Engg. 2022, 2, 110−120

28.3% at 160 °C. The weight of PET was reduced by 35.0% after the oxidation (Figure 3a), while 24.8% PET could be decomposed with 0.2 M H^+ (without Fe^{2+}/H_2O_2), as shown in Figure 3b, indicating the low reactivity of PET with Fenton's reagent. This can be attributed to the high melting point of PET, which is above 225 °C. On the whole, the thermal Fenton system is effective to treat most types of MPs that are commonly detected in the environment.

MP Characterizations Before and After Thermal Fenton Processes. Figure 4 shows the morphological changes of MPs after different time spans of the Fenton reaction. Figure 4a shows the original MPs before reactions. After 2 h of Fenton treatment (Figure 4b), MPs started to aggregate into larger pieces. When the reaction proceeded for 4 h (Figure 4c), MPs were fused into flat layers and small holes appeared on the surface, which was caused by the Fenton oxidation process or MP contraction upon cooling to room temperature. After 6 h of oxidation (Figure 4d), a few larger holes (up to 10 μm) emerged on the rough surface, indicating that MPs were decomposed, which corresponds to the apparent weight loss after 6 h treatment shown in Figure 1. Larger cavities were found on the plastics as the treatment time increased to 8 h (Figure 4e). When it comes to 12 h, the MPs were fragmented into smaller particles (Figure 4f). However, due to the MP aggregation in the first 4 h, a large number of fragmented residues were still larger than the original particles (Figure S3a,b). SEM images with larger scales are shown in Figure S4 to show the full picture of the aggregated particles.

FTIR analysis was performed to observe the changes in the chemical property of MPs after the oxidation (Figure 5). The peaks at 2915 and 2847 cm^{-1} correspond to the asymmetric and symmetric stretching vibrations of the CH_2 group, respectively, and the peak at 719 cm^{-1} represents the rocking deformation of C−H (Figure 5a).[45−47] The peaks at 1473 and 1463 cm^{-1} represent the bending deformation of CH_2 and CH_3, respectively.[45] The broad peak in the range of 3600−3300 cm^{-1} stands for the stretching vibration of O−H, and the broad peak below 2915 and 2847 cm^{-1} between 3000 and 2500 cm^{-1} represents the O−H bond in the carboxylic group.[48,49] The peak that emerged at 1706 cm^{-1} after the reaction contributes to the stretching vibration of the C═O group in the carboxylic acid or ketone moiety.[47] Another new peak at 1165 cm^{-1} stands for the stretching vibration of C−O.[46] More details of each bond and the corresponding frequency changes are given in Tables S2 and S3.

In comparison with the untreated PE (Figure 5b), MPs after Fenton oxidation showed several significant changes in FTIR. Specifically, the peak intensity of both C═O and C−O groups appeared and dramatically increased during the treatment, while the peak of C−O−C in carbon branches did not appear at 1103 cm^{-1} until being oxidized for 6 h. The broad peak between 3600 and 3300 cm^{-1} represents hydroxyl groups with hydrogen bonds. It is also reported that the broad peak between 3000 and 2500 cm^{-1} and the strong peak at 1410 cm^{-1} can certify the existence of carboxylic acid groups.[49] The appearances of the abovementioned oxygen groups indicate oxidation of MPs during the thermal Fenton treatment. These oxygenated groups have been reported to accelerate the degradation of MPs because the hydroxyl groups are more facile to be oxidized by $^{\bullet}OH$.[50] In terms of CH_2 bonds at 2915 and 2847 cm^{-1}, despite that they seemed to experience extraordinary changes after oxidation, the broad O−H peak under these peaks increased the baseline and the addition of carbonyl groups increased the CH_2 peak intensity of the adjacent methylene group.[49,51] Therefore, it is difficult to qualitatively analyze the changes in the number of methylene and methyl groups. However, the peaks representing CH_3 symmetric deformation at 1372 cm^{-1} rose as oxidation continued, which demonstrates the breakup of carbon chains and increased exposure of CH_3 after oxidation. In addition, by comparing the bond positions at different time intervals, all vibrations related to C−H shifted to higher positions except the peaks of out-plane CH_2 vibrations, and the peaks of C═O and C−O−C shifted to lower frequencies. This phenomenon may be caused by the substitution of functional groups along the carbon chains.[49] Specifically, the frequency of methyl usually increases when the associated carbon atom connects to oxygen, and C═C bonds tend to lower the frequency of carbonyl groups due to the conjugate effects.[49] Moreover, we can qualitatively assess the crystallinity of MPs by analyzing the peaks at 1473 and 1463 cm^{-1}, according to the empirical equation given below (eq 2)[52]

$$X = \frac{((1 - I_a/I_b)/1.233)}{1 + I_a/I_b} \times 100 \quad (2)$$

where X is the percent fraction of amorphous material and I_a and I_b are the intensity of peaks 1473 and 1463 cm^{-1}, respectively. In Figure S5a, the intensity ratio of I_a/I_b decreased after thermal Fenton treatment, and thus the amorphous portion of MPs was augmented. This may be caused by the addition of oxygen atoms, which would increase the steric hindrance and hinder the carbon chain from aligning orderly via hydrogen bonding, giving rise to decreased crystallinity of MPs. The red shift of carbonyl stretching at 1705−1713 cm^{-1} evidences the formation of a hydrogen bond, and the consequent lower crystallinity also complies with the previous study.[53]

For the structural changes due to Fenton oxidation, DSC was carried out to calculate the changes of crystallinity. The degree of crystallinity is defined as follows (eq 3)[54]

$$X_c = \Delta H_f(T_m)/\Delta H_f^0(T_m^0) \quad (3)$$

where X_c is the degree of crystallinity in weight; $\Delta H_f(T_m)$ is the enthalpy of fusion measured at melting temperature, T_m; and $\Delta H_f^0(T_m^0)$ is the corresponding enthalpy of totally crystalline UHMWPE, which usually is 293 J g^{-1}.[55] The DSC curves of MPs after different time spans of oxidation are shown in Figure S6, and the calculated degree of crystallinity increased between 0 and 2 h, as shown in Table 1. When the system cooled slowly from the hydrothermal condition (140 °C), the more stretching carbon chains at the second hour are prone to align orderly to form a crystalline phase instead of an amorphous phase.[56] Also, the ruptures of carbon chains in the amorphous phase usually facilitate the formation of a crystalline phase due to the chemicrystallization process.[57] Thus, the crystallinity increased in the first 2 h. At this stage, the level of generated carbonyl groups was not high enough to intervene in the crystallization process. On the other side, the

Table 1. Calculated Results from DSC Analysis

time (h)	0	2	4	6	8
enthalpy (J g^{-1})	218	236	152	44.4	11.1
crystallinity (%)	74.4	80.6	51.9	15.2	3.8

https://doi.org/10.1021/acsestengg.1c00323
ACS EST Engg. 2022, 2, 110−120

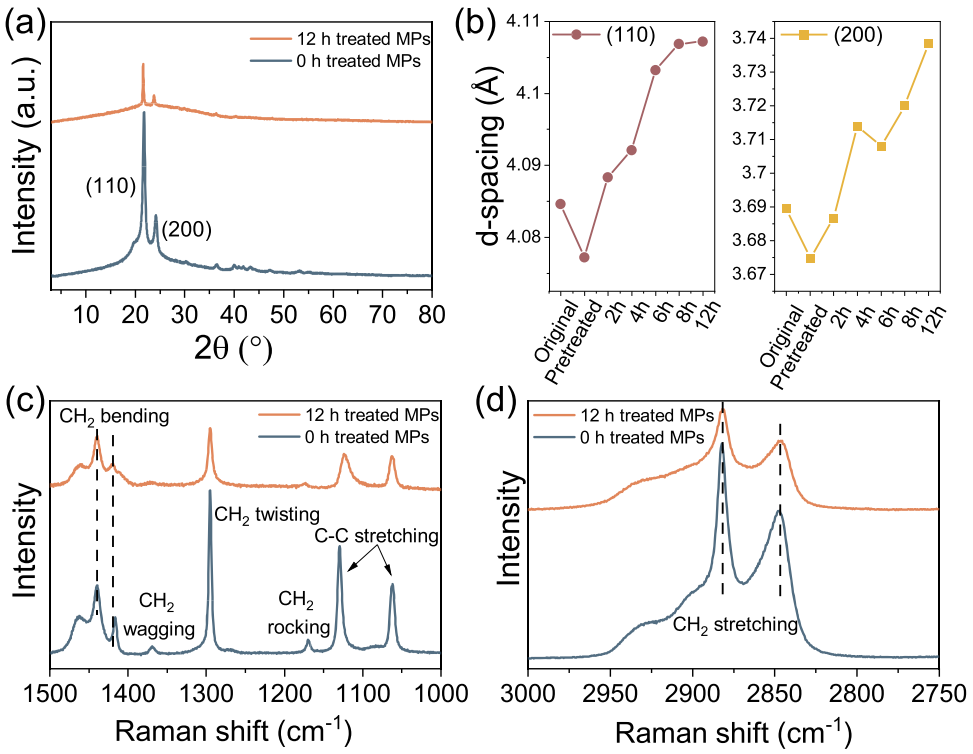

Figure 6. (a) XRD patterns of treated and untreated MPs, (b) calculated *d*-spacing of MPs after different times of Fenton treatment, and Raman spectra of MPs after Fenton treatment at (c) 1500−1000 cm^{-1} and (d) 3000−2750 cm^{-1} (Fe^{2+}: 4 mM, H_2O_2: 200 mM, UHMWPE MPs: 1 g L^{-1}, time: 12 h, temperature: 140 °C).

crystallinity decreased from 2 to 8 h. During this process, the oxidation somehow prohibited the crystallization, which reflects the increased irregularity of carbon chains caused by the additional carbonyl groups. Thus, the decreased crystallinity between 2 and 8 h indicates that the newly formed carbonyl groups inhibit the recrystallization process due to the steric hindrance.

XRD patterns of the crystal structures of MPs during the oxidation are shown in Figure 6a,b to monitor the changes in the crystal structures of MPs over time. Both the MPs before and after Fenton treatment have two main characteristic peaks, which correspond to the (110) and (200) reflections, indicating the orthorhombic structure of crystal PE polymers.[58] Compared to the untreated MPs, lower peak intensities of treated MPs indicate a decreased degree of crystallinity, which consents to the DSC results. For the (110) reflection, after a time span of reaction, the peak shifted from 21.74 to 21.62°. According to Bragg's law, the interplanar spacing of the (110) and (200) reflections gradually increased from 4.09 to 4.11 Å and from 3.69 to 3.74 Å, respectively, at extended reaction time. The increase in interplanar spacing was caused by the formation of carbonyl or hydroxyl groups on the sides of carbon chains. When the temperature cools to room temperature after the reaction, the carbon chains tend to fold together and reform ordered regions.[59] During this process, the newly formed carbonyl groups, as revealed by FTIR in Figure 5, would restrain the stretched carbon chains to form compact structures due to the steric hindrance, thus increasing the interplanar spacing and ultimately decreasing the proportion of the crystal phase. In addition, the formation of oxidized carbon segments due to the scissoring of a macromolecule may also contribute to the larger interplanar spacing.

Raman spectra were recorded to analyze the molecular structures of MPs, such as the degree of crystallinity and density during the degradation process. The full-range surveys of MPs after different stages of oxidation are displayed in Figure S7, and corresponding assignments of Raman bands are summarized in Table S4. According to Figure 6c, in the CH_2 bending region, the intensity ratio of the CH_2 (crystalline) bending vibration at 1416 cm^{-1} vs the CH_2 (amorphous) at 1439 cm^{-1} became lower after the thermal Fenton process. This lower intensity signifies the inferior degree of crystallinity, which also implies the lower density of MPs.[60] This result is consistent with the previous report using peaks at 1416 and 1439 cm^{-1} to determine the crystalline and amorphous phases.[61−63] Similar conclusions can be obtained in the CH_2 stretching region (Figure 6d). The increased intensity ratio of the symmetric CH_2 stretching mode at 2847 cm^{-1} vs the asymmetric CH_2 stretching mode at 2882 cm^{-1} unveiled the lower density of MPs.[60] Compared with the untreated MPs, MPs that experienced a 12 h Fenton reaction exhibited lower peak intensities of all forms of CH_2 vibration (Figure 6c,d), indicating the decreased number of CH_2 groups. This can be ascribed to the breakup of carbon chains and the substitution of hydrogen by oxygen during oxidation. In addition, a new peak emerged at 1740 cm^{-1} after the reaction (Figure S7b), which represents the stretching vibrations of carbonyl groups.[62] Compared with the FTIR spectra, the C═O peak is unnoticeable because the signal of the carbonyl group is typically weak in Raman spectroscopy. This phenomenon indicates the generation of C═O and oxidation of MPs, which is in good agreement with the results of FTIR. The appearance of the peak at 904 cm^{-1} after Fenton treatment demonstrates that a small number of broken carbon chains were formed after oxidation (Figure S7c).[61]

https://doi.org/10.1021/acsestengg.1c00323
ACS EST Engg. 2022, 2, 110−120

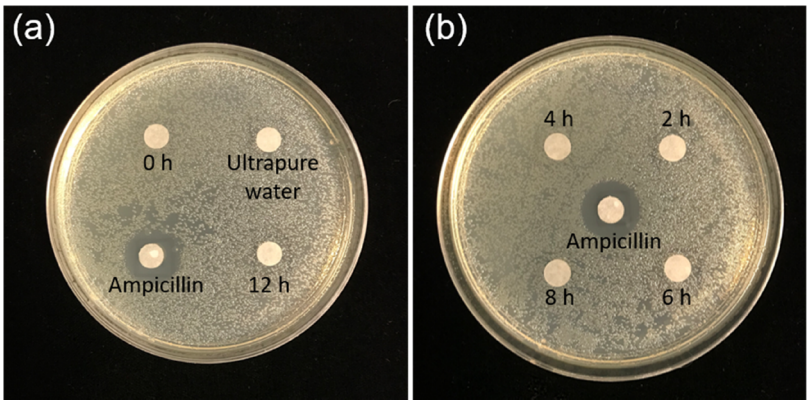

Figure 7. Toxicity evaluation results of solutions: (a) ultrapure water, ampicillin, 0 and 12 h reaction filtrate and (b) 2, 4, 6, and 8 h reaction filtrates.

Figure S8 shows the XPS survey of original MPs, pretreated MPs (initial), and 8 h Fenton-treated MPs. The pretreated MPs showed C 1s and O 1s peaks with corresponding contents of 89.2 and 10.8 at. %, respectively. In contrast, the oxygen content in MPs increased to 19.8 at. % after 8 h oxidation, which agrees with the outcomes of FTIR and Raman. The increased O/C ratio indicates the higher hydrophilicity of MPs.[35] Furthermore, the C 1s peaks were fitted into four components with peaks at 284.5, 286.3, 287.3, and 289.0 eV, corresponding to the carbons in C−C, C−OH/C−O−C, C═O, and O−C═O, respectively. After thermal Fenton treatment, the contents of C−OH/C−O−C and O−C═O distinctly increased after the reaction. However, the peak area of C═O slightly dropped after Fenton oxidation. Combining the results of FTIR spectra shown in Figure 5, the C═O peak that emerged at 1706 cm^{-1} was mainly ascribed to carboxylic acid or ester instead of a ketone moiety or an aldehyde group. The results suggest that oxidation prefers to occur at the ends of carbon chains to form carboxylic acid. Considering the slight reduction of the C═O peak in the XPS analysis, the ketone moiety formed on the carbon chain is susceptible to be further oxidized into an ester or a carboxylic acid group via C−C bond scission. There was no C═C peak detected in the XPS survey, which agrees with the tiny Raman peak at 1640 cm^{-1} (Figure S7b).[49] The small amount of C═C indicates that the double bond may experience further oxidation or oxidative cleavage into small molecules. In addition, due to the presence of HCl, chlorine radicals with mild oxidation potentials might be produced and cause surface chlorination of MPs or chlorinated byproducts. However, no obvious peak for the Cl element (~200 eV) was observed in the XPS spectra (Figure S10a).[64] So the chlorinated MPs might not exist or surface chlorinated groups are at a trace level below the detection limit.

Effects of Pretreatment with NaOH. NaOH can react with oxygen-containing groups on PE to obtain pristine MPs.[65] The absence of functional groups will help to investigate the behaviors of unaged MPs. Also, in a previous study,[66,67] high-concentration NaOH was utilized for pretreatment of plastics, which successfully increased the photoreforming performance. The NaOH hydrolysis generated monomers of ethylene glycol from PET as a reactant for photoreforming to enhance the initial rate of H_2 production. The performance comparison of thermal Fenton oxidation with and without pretreatment is shown in Figure 3a. Compared with the original MPs, the weight loss of the pretreated MPs slightly decreased by 5%. By comparing the FTIR spectra (Figure S5b), the broad peak at 1200−1000 cm^{-1} disappeared after NaOH hydrolysis, indicating that NaOH would react with the oxygen-containing groups on MPs, which is consistent with a previous study that NaOH reduced the oxygen content and removed carboxylic acid groups.[65] Therefore, the polymer carbon chains experienced reduction reactions with NaOH, and the reduced oxygen may slow down the initial rate of oxidation. The presence of oxygen-containing groups can increase the hydrophilicity of MPs, thus enhancing the contact reaction with ROS.[50,64] Also, the existence of oxygen may contribute to the formation of oxygen-containing radicals such as $CO^{\bullet}$ (tertiary alkoxy radicals), which will, in turn, attack the polymer and cause chain breakdown.[68] A similar phenomenon was observed in XPS spectra (Figure S8). The total oxygen content was distinctly reduced from 16.3% to 10.8 at. % after pretreatment. According to the C 1s peak deconvolution, the contents of all forms of carbon−oxygen bonds decreased by certain degrees. This proves that the higher incipient oxygen content has a promotion effect on thermal Fenton oxidation. In addition, XRD demonstrates the structural change caused by NaOH hydrolysis (Figure 6b). The *d*-spacing of both (110) and (200) decreased from 4.085 to 4.077 and 3.690 to 3.675 Å after the pretreatment, respectively. Considering the results of FTIR and XPS, the decline in the oxygen content after hydrolysis will cause a more compact crystalline structure of MPs. Therefore, the greater crystallinity may be another reason for the inferior oxidation of the pretreated samples because a longer treatment time is required to fully extend the polymer carbon chains, which reduced the valid time for ROS to attack the macromolecules. Thus, NaOH pretreatment is beneficial in photoreforming of PET but not in thermal Fenton oxidation of UHMWPE.

Performance in Real Water Matrices and Daily-Life MPs. To investigate the influence of the water matrix, we also carried out MP degradations in tap water, river water, and seawater (Figure S9). All of the three matrices have limited inhibitory effects on the degradation efficiency, indicating the high adaptability of the thermal Fenton system for treating MPs in natural water bodies. Interestingly, MP degradation in seawater was faster than ultrapure water, which may be ascribed to the chlorine-based radicals formed in seawater of high salinity. The oxidation of typical real-life plastics was also evaluated (Figure S10). For the plastic beads in facial scrub (LDPE), plastic bags (LDPE), and wrap films (LDPE), the degradation efficiency can reach above 85%. But the thermal

https://doi.org/10.1021/acsestengg.1c00323
ACS EST Engg. 2022, 2, 110−120

Fenton is not effective to the debris from a milk bottle (HDPE). Some additives such as plasticizers, stabilizers, and antioxidants are added to commercial plastics to increase their stability and make them more stubborn to degrade.[69] Therefore, the differences in MP deformation might be caused by the texture, surface area, additives, and melting points.

Toxicity Evaluation. During MP degradation in thermal Fenton processes, various hydrocarbon intermediates may be generated in the solution. Thus, the potential risk of the resulted solution was evaluated via a filter paper disk method using *E. coli*. The growth of *E. coli* in agar plates is shown in Figure 7. Normally, if the inhibition zone appears around ampicillin, the growth of *E. coli* is restrained, which implies that the substance in filter paper is toxic or unfavorable for *E. coli* growth. Thus, the absence of the inhibition zone for filtrates obtained after different hours of Fenton treatment indicates that the filtrates are benign to *E. coli* growth.[36,37] In other words, the intermediates generated during Fenton treatment are nontoxic to *E. coli*. Notably, before commencing toxicity tests, pH neutralization was required. Such a process would result in slight iron sludge flocculation that might contain some intermediates, which also reduced the toxicity of the filtrate.

Environmental Implications. In an aqueous environment, MPs can cause potential physical injuries to microorganisms and act as carriers of detrimental pollutants. Even though current advanced WWTPs can retain over 98% MPs, extremely large quantities of MPs are still released into water bodies. Effective technologies including microwaves, biodegradation, and photocatalysis are either mainly focused on solid-state plastics or suffering from low degradation rates. Effective MP remediation strategies in an aqueous environment are critically required to keep water security from MP pollution. This work integrated Fenton's reagent and a hydrothermal condition for efficient degradation of MPs in water. The synergistic effects of Fenton's reagent, protons, and hydrothermal conditions promoted the degradation of MPs with different textures and particle sizes. Thus, the hydrothermal Fenton process can be integrated into the tertiary treatment in WWTPs to simultaneously remove trace-level MPs, organic pollutants, and microorganisms, which cannot be achieved by solid-state-based technologies. In this study, a two-stage oxidation process was found for UHMWPE oxidation, where MPs extended their carbon chain in the first stage and started to decompose to generate a large number of C═O and C−O groups in the second stage. Operation temperature that is close to the melting point of the MPs is vital for carbon chain extension. The degree of crystallinity and density decreased as the thermal Fenton reaction proceeded, and the system did not release toxic intermediates. Not only PE, but the thermal Fenton technology was also capable to degrade common petroleum-based plastics (PP, PVC, and PS). To our delight, the system was also effective in MP removals in real-life water bodies. The discovery in this study is of critical importance to current MP removal strategies as it has the virtue of high efficiency, low toxicity, and effectiveness in an aqueous environment. Future research opportunities can be the development of Fenton-like systems for MP remediation with greater applicability with a broader pH working window, lower reaction temperature, and reduced oxidant usage.

■ ASSOCIATED CONTENT

Supporting Information

The Supporting Information is available free of charge at https://pubs.acs.org/doi/10.1021/acsestengg.1c00323.

Calculation of the mineralization rate; equations of H_2O_2 quenching and plastic decomposition; the first-order kinetic fitting of the system; degradation of MPs with PMS and PDS homogeneous systems; degradation efficiency of different types of MPs; size distribution of the MPs and cavities appeared on the MPs after degradation; FTIR spectra, DSC profiles, Raman spectra, and XPS surveys of MPs; degradation performance under real-life water bodies; degradation performance toward real-life MPs; toxicity evaluation of filtrate; and band assignments of FTIR and Raman spectra (PDF)

■ AUTHOR INFORMATION

Corresponding Authors

Xiaoguang Duan − *School of Chemical Engineering and Advanced Materials, The University of Adelaide, Adelaide, SA 5005, Australia*; orcid.org/0000-0001-9635-5807; Email: xiaoguang.duan@adelaide.edu.au

Shaobin Wang − *School of Chemical Engineering and Advanced Materials, The University of Adelaide, Adelaide, SA 5005, Australia*; orcid.org/0000-0002-1751-9162; Email: shaobin.wang@adelaide.edu.au

Authors

Kunsheng Hu − *School of Chemical Engineering and Advanced Materials, The University of Adelaide, Adelaide, SA 5005, Australia*

Peng Zhou − *College of Architecture & Environment, Sichuan University, Chengdu 610065, P. R. China*

Yangyang Yang − *School of Chemical Engineering and Advanced Materials, The University of Adelaide, Adelaide, SA 5005, Australia*

Tony Hall − *School of Sciences, The University of Adelaide, Adelaide, SA 5005, Australia*

Gang Nie − *Department of Environmental Science and Engineering, Wuhan University, Wuhan 430079, P. R. China*

Yu Yao − *School of Chemical Engineering and Advanced Materials, The University of Adelaide, Adelaide, SA 5005, Australia*

Complete contact information is available at: https://pubs.acs.org/10.1021/acsestengg.1c00323

Notes

The authors declare no competing financial interest.

■ ACKNOWLEDGMENTS

The authors acknowledge the financial support from the Australian Research Council (DP200103206). In addition, K.H. especially acknowledges Prof. Iain Searle for his professional assistance in *E. coli* cultivation for toxicity evaluation.

■ REFERENCES

(1) PlasticsEurope Plastics − the Facts 2020. An analysis of European plastics production, demand and waste data. https://www.plasticseurope.org/en/resources/publications/4312-plastics-facts-2020 (accessed June 25, 2021).

(2) Geyer, R.; Jambeck, J. R.; Law, K. L. Production, use, and fate of all plastics ever made. *Sci. Adv.* **2017**, *3*, No. e1700782.
(3) Nguyen, B.; Claveau-Mallet, D.; Herandez, L. M.; Xu, E. G.; Farner, J. M.; Tufenkji, N. Separation and analysis of microplastics and nanoplastics in complex environmental samples. *Acc. Chem. Res.* **2019**, *52*, 858−866.
(4) Fendall, L. S.; Sewell, M. A. Contributing to marine pollution by washing your face: microplastics in facial cleansers. *Mar. Pollut. Bull.* **2009**, *58*, 1225−1228.
(5) Xue, B. M.; Zhang, L. L.; Li, R. L.; Wang, Y. H.; Guo, J.; Yu, K. F.; Wang, S. P. Underestimated microplastic pollution derived from fishery activities and "hidden" in deep sediment. *Environ. Sci. Technol.* **2020**, *54*, 2210−2217.
(6) Eerkes-Medrano, D.; Thompson, R. C.; Aldridge, D. C. Microplastics in freshwater systems: a review of the emerging threats, identification of knowledge gaps and prioritisation of research needs. *Water Res.* **2015**, *75*, 63−82.
(7) Andrady, A. L. Microplastics in the marine environment. *Mar. Pollut. Bull.* **2011**, *62*, 1596−1605.
(8) Horton, A. A.; Walton, A.; Spurgeon, D. J.; Lahive, E.; Svendsen, C. Microplastics in freshwater and terrestrial environments: evaluating the current understanding to identify the knowledge gaps and future research priorities. *Sci. Total Environ.* **2017**, *586*, 127−141.
(9) Zhang, Q.; Xu, E. G.; Li, J.; Chen, Q.; Ma, L.; Zeng, E. Y.; Shi, H. A review of microplastics in table salt, drinking water, and air: direct human exposure. *Environ. Sci. Technol.* **2020**, *54*, 3740−3751.
(10) Lusher, A. L.; Tirelli, V.; O'Connor, I.; Officer, R. Microplastics in Arctic polar waters: the first reported values of particles in surface and sub-surface samples. *Sci. Rep.* **2015**, *5*, No. 14947.
(11) Waller, C. L.; Griffiths, H. J.; Waluda, C. M.; Thorpe, S. E.; Loaiza, I.; Moreno, B.; Pacherres, C. O.; Hughes, K. A. Microplastics in the Antarctic marine system: an emerging area of research. *Sci. Total Environ.* **2017**, *598*, 220−227.
(12) Hernandez, L. M.; Xu, E. G.; Larsson, H. C. E.; Tahara, R.; Maisuria, V. B.; Tufenkji, N. Plastic teabags release billions of microparticles and nanoparticles into tea. *Environ. Sci. Technol.* **2019**, *53*, 12300−12310.
(13) Kniggendorf, A. K.; Wetzel, C.; Roth, B. Microplastics detection in streaming tap water with Raman spectroscopy. *Sensors* **2019**, *19*, No. 1839.
(14) Oßmann, B. E.; Sarau, G.; Holtmannspötter, H.; Pischetsrieder, M.; Christiansen, S. H.; Dicke, W. Small-sized microplastics and pigmented particles in bottled mineral water. *Water Res.* **2018**, *141*, 307−316.
(15) Kutralam-Muniasamy, G.; Pérez-Guevara, F.; Elizalde-Martínez, I.; Shruti, V. C. Branded milks - Are they immune from microplastics contamination? *Sci. Total Environ.* **2020**, *714*, No. 136823.
(16) Lebreton, L.; Andrady, A. Future scenarios of global plastic waste generation and disposal. *Palgrave Commun.* **2019**, *5*, No. 6.
(17) Burgess, R. M.; Ho, K. T.; et al. The challenge: microplastics in the aquatic environment-Perspectives on the scope of the problem. *Environ. Toxicol. Chem.* **2017**, *36*, 2259.
(18) Wright, S. L.; Thompson, R. C.; Galloway, T. S. The physical impacts of microplastics on marine organisms: a review. *Environ. Pollut.* **2013**, *178*, 483−492.
(19) Rochman, C. M.; Browne, M. A.; Halpern, B. S.; Hentschel, B. T.; Hoh, E.; Karapanagioti, H. K.; Rios-Mendoza, L. M.; Takada, H.; Teh, S.; Thompson, R. C. Classify plastic waste as hazardous. *Nature* **2013**, *494*, 169−171.
(20) Cole, M.; Lindeque, P.; Halsband, C.; Galloway, T. S. Microplastics as contaminants in the marine environment: a review. *Mar. Pollut. Bull.* **2011**, *62*, 2588−2597.
(21) Pauly, J. L.; Stegmeier, S. J.; Allaart, H. A.; Cheney, R. T.; Zhang, P. J.; Mayer, A. G.; Streck, R. J. Inhaled cellulosic and plastic fibers found in human lung tissue. *Cancer Epidemiol., Biomarkers Prev.* **1998**, *7*, 419−428.
(22) Schwabl, P.; Köppel, S.; Königshofer, P.; Bucsics, T.; Trauner, M.; Reiberger, T.; Liebmann, B. Detection of various microplastics in human stool a prospective case series. *Ann. Intern. Med.* **2019**, *171*, 453−457.
(23) Hu, K.; Tian, W.; Yang, Y.; Nie, G.; Zhou, P.; Wang, Y.; Duan, X.; Wang, S. Microplastics remediation in aqueous systems: strategies and technologies. *Water Res.* **2021**, *198*, No. 117144.
(24) Tavares, R.; Ramos, A.; Rouboa, A. Microplastics thermal treatment by polyethylene terephthalate-biomass gasification. *Energy Convers. Manage.* **2018**, *162*, 118−131.
(25) Cheng, L. L.; Gu, J.; Wang, Y. Z.; Zhang, J.; Yuan, H. R.; Chen, Y. Polyethylene high-pressure pyrolysis: better product distribution and process mechanism analysis. *Chem. Eng. J.* **2020**, *385*, No. 123866.
(26) Jie, X.; Li, W.; Slocombe, D.; Gao, Y.; Banerjee, I.; Gonzalez-Cortes, S.; Yao, B.; AlMegren, H.; Alshihri, S.; Dilworth, J.; Thomas, J.; Xiao, T.; Edwards, P. Microwave-initiated catalytic deconstruction of plastic waste into hydrogen and high-value carbons. *Nat. Catal.* **2020**, *3*, 902−912.
(27) Lares, M.; Ncibi, M. C.; Sillanpää, M.; Sillanpää, M. Occurrence, identification and removal of microplastic particles and fibers in conventional activated sludge process and advanced MBR technology. *Water Res.* **2018**, *133*, 236−246.
(28) Ye, H.; Wang, Y.; Liu, X.; Xu, D.; Yuan, H.; Sun, H.; Wang, S.; Ma, X. Magnetically steerable iron oxides-manganese dioxide core−shell micromotors for organic and microplastic removals. *J. Colloid Interface Sci.* **2021**, *588*, 510−521.
(29) Kang, J.; Zhou, L.; Duan, X. G.; Sun, H. Q.; Ao, Z. M.; Wang, S. B. Degradation of cosmetic microplastics via functionalized carbon nanosprings. *Matter* **2019**, *1*, 745−758.
(30) Miao, F.; Liu, Y.; Gao, M.; Yu, X.; Xiao, P.; Wang, M.; Wang, S.; Wang, X. Degradation of polyvinyl chloride microplastics via an electro-Fenton-like system with a TiO_2/graphite cathode. *J. Hazard. Mater.* **2020**, *399*, No. 123023.
(31) Wang, N. N.; Zheng, T.; Zhang, G. S.; Wang, P. A review on Fenton-like processes for organic wastewater treatment. *J. Environ. Chem. Eng.* **2016**, *4*, 762−787.
(32) Tagg, A. S.; Harrison, J. P.; Ju-Nam, Y.; Sapp, M.; Bradley, E. L.; Sinclair, C. J.; Ojeda, J. J. Fenton's reagent for the rapid and efficient isolation of microplastics from wastewater. *Chem. Commun.* **2017**, *53*, 372−375.
(33) Hurley, R. R.; Lusher, A. L.; Olsen, M.; Nizzetto, L. Validation of a method for extracting microplastics from complex, organic-rich, environmental matrices. *Environ. Sci. Technol.* **2018**, *52*, 7409−7417.
(34) Masura, J.; Baker, J. E.; Foster, G. D.; Arthur, C.; Herring, C. Laboratory methods for the analysis of microplastics in the marine environment: recommendations for quantifying synthetic particles in waters and sediments. https://marinedebris.noaa.gov/sites/default/files/publications-files/noaa_microplastics_methods_manual.pdf (accessed June 22, 2021).
(35) Liu, P.; Qian, L.; Wang, H. Y.; Zhan, X.; Lu, K.; Gu, C.; Gao, S. X. New insights into the aging behavior of microplastics accelerated by advanced oxidation processes. *Environ. Sci. Technol.* **2019**, *53*, 3579−3588.
(36) Mohan, H.; Ramasamy, M.; Ramalingam, V.; Natesan, K.; Duraisamy, M.; Venkatachalam, J.; Shin, T.; Seralathan, K. K. Enhanced visible light-driven photocatalysis of iron-oxide/titania composite: norfloxacin degradation mechanism and toxicity study. *J. Hazard. Mater.* **2021**, *412*, No. 125330.
(37) Tether, A. L.; Laverty, G.; Puga, A. V.; Seddon, K. R.; Gilmore, B. F.; Kelly, S. A. High-throughput toxicity screening of novel azepanium and 3-methylpiperidinium ionic liquids. *RSC Adv.* **2020**, *10*, 22864−22870.
(38) Zhang, M. H.; Dong, H.; Zhao, L.; Wang, D. X.; Meng, D. A review on Fenton process for organic wastewater treatment based on optimization perspective. *Sci. Total Environ.* **2019**, *670*, 110−121.
(39) Hodaifa, G.; Ochando-Pulido, J. M.; Rodriguez-Vives, S.; Martinez-Ferez, A. Optimization of continuous reactor at pilot scale for olive-oil mill wastewater treatment by Fenton-like process. *Chem. Eng. J.* **2013**, *220*, 117−124.

https://doi.org/10.1021/acsestengg.1c00323
ACS EST Engg. 2022, 2, 110−120

(40) Pignatello, J. J.; Oliveros, E.; MacKay, A. Advanced oxidation processes for organic contaminant destruction based on the Fenton reaction and related chemistry. *Crit. Rev. Environ. Sci. Technol.* **2006**, *36*, 1−84.
(41) Bandura, A. V.; Lvov, S. N. The ionization constant of water over wide ranges of temperature and density. *J. Phys. Chem. Ref. Data* **2006**, *35*, 15−30.
(42) Nieto, L. M.; Hodaifa, G.; Rodríguez, S.; Giménez, J. A.; Ochando, J. Degradation of organic matter in olive-oil mill wastewater through homogeneous Fenton-like reaction. *Chem. Eng. J.* **2011**, *173*, 503−510.
(43) Ariza-Tarazona, M. C.; Villarreal-Chiu, J. F.; Hernández-López, J. M.; De la Rosa, J. R.; Barbieri, V.; Siligardi, C.; Cedillo-González, E. I. Microplastic pollution reduction by a carbon and nitrogen-doped TiO_2: effect of pH and temperature in the photocatalytic degradation process. *J. Hazard. Mater.* **2020**, *395*, No. 122632.
(44) De Laat, J.; Le, T. G. Effects of chloride ions on the iron(III)-catalyzed decomposition of hydrogen peroxide and on the efficiency of the Fenton-like oxidation process. *Appl. Catal., B* **2006**, *66*, 137−146.
(45) Gulmine, J. V.; Janissek, P. R.; Heise, H. M.; Akcelrud, L. Polyethylene characterization by FTIR. *Polym. Test.* **2002**, *21*, 557−563.
(46) Ali, S. S.; Qazi, I. A.; Arshad, M.; Khan, Z.; Voice, T. C.; Mehmood, C. T. Photocatalytic degradation of low density polyethylene (LDPE) films using titania nanotubes. *Environ, Nanotechnol., Monit. Manage.* **2016**, *5*, 44−53.
(47) Dang, T. H. D.; Nguyen, D.; Thai, H.; Nguyen, T.; Tran, T.; Le, H.; Nguyen, V.; Tran, X.; Pham, T.; Nguyen, T.; Quang Trung, N. Plastic degradation by thermophilic *Bacillus* sp. BCBT21 isolated from composting agricultural residual in Vietnam. *Adv. Nat. Sci.: Nanosci. Nanotechnol.* **2018**, *9*, No. 015014.
(48) Celia, E.; de Givenchy, E. T.; Amigoni, S.; Guittard, F. Three steps to organic−inorganic hybrid films showing superhydrophilic properties. *Soft Matter* **2011**, *7*, 10057−10062.
(49) Bellamy, L. *The Infra-Red Spectra of Complex Molecules*; Springer Science & Business Media: New York, 2013.
(50) Wang, C.; Xian, Z.; Jin, X.; Liang, S.; Chen, Z.; Pan, B.; Wu, B.; Ok, Y. S.; Gu, C. Photo-aging of polyvinyl chloride microplastic in the presence of natural organic acids. *Water Res.* **2020**, *183*, No. 116082.
(51) Francis, S. A. Intensities of some characteristic infrared bands of ketones and esters. *J. Chem. Phys.* **1951**, *19*, 942−948.
(52) Zerbi, G.; Gallino, G.; Del Fanti, N.; Baini, L. Structural depth profiling in polyethylene films by multiple internal reflection infra-red spectroscopy. *Polymer* **1989**, *30*, 2324−2327.
(53) Shi, J. J.; Wang, W.; Feng, Z. H.; Zhang, D. H.; Zhou, Z.; Li, Q. F. Multiple influences of hydrogen bonding interactions on PLLA crystallization behaviors in PLLA/TSOS hybrid blending systems. *Polymer* **2019**, *175*, 152−160.
(54) Kong, Y.; Hay, J. N. The measurement of the crystallinity of polymers by DSC. *Polymer* **2002**, *43*, 3873−3878.
(55) Simis, K. S.; Bistolfi, A.; Bellare, A.; Pruitt, L. A. The combined effects of crosslinking and high crystallinity on the microstructural and mechanical properties of ultra high molecular weight polyethylene. *Biomaterials* **2006**, *27*, 1688−1694.
(56) Richards, R. B. Polyethylene-structure, crystallinity and properties. *J. Appl. Chem.* **1951**, *1*, 370−376.
(57) Arhant, M.; Le Gall, M.; Le Gac, P. Y.; Davies, P. Impact of hydrolytic degradation on mechanical properties of PET - Towards an understanding of microplastics formation. *Polym. Degrad. Stab.* **2019**, *161*, 175−182.
(58) Wang, F.; Liu, L. C.; Xue, P.; Jia, M. Y.; Wang, S. W.; Cai, J. C. The influence of formation temperatures on the crystal structure and mechanical properties of ultrahigh-molecular-weight polyethylene/high-density polyethylene-blend fibers prepared by melt spinning. *J. Ind. Text.* **2020**, *49*, 1011−1035.
(59) Lankone, R. S.; Wang, J. J.; Ranville, J. F.; Fairbrother, D. H. Photodegradation of polymer-CNT nanocomposites: effect of CNT loading and CNT release characteristics. *Environ. Sci.: Nano* **2017**, *4*, 967−982.
(60) Ibrahim, M.; He, H. Classification of polyethylene by Raman spectroscopy. https://assets.thermofisher.com/TFS-Assets/MSD/Application-Notes/AN52301-classification-polyethylene-Raman-spectroscopy-app-note.pdf (accessed June 18, 2021).
(61) Sato, H.; Shimoyama, M.; Kamiya, T.; Amari, T.; Šašic, S.; Ninomiya, T.; Siesler, H. W.; Ozaki, Y. Raman spectra of high-density, low-density, and linear low-density polyethylene pellets and prediction of their physical properties by multivariate data analysis. *J. Appl. Polym. Sci.* **2002**, *86*, 443−448.
(62) Strobl, G. R.; Hagedorn, W. Raman spectroscopic method for determining the crystallinity of polyethylene. *J. Polym. Sci., Polym. Phys. Ed.* **1978**, *16*, 1181−1193.
(63) Barron, D.; Birkinshaw, C. Ultra-high molecular weight polyethylene - Evidence for a three-phase morphology. *Polymer* **2008**, *49*, 3111−3115.
(64) Zhou, L.; Wang, T.; Qu, G.; Jia, H.; Zhu, L. Probing the aging processes and mechanisms of microplastic under simulated multiple actions generated by discharge plasma. *J. Hazard. Mater.* **2020**, *398*, No. 122956.
(65) Terlingen, J. G. A.; Gerritsen, H. F. C.; Hoffman, A. S.; Jen, F. J. Introduction of functional groups on polyethylene surfaces by a carbon dioxide plasma treatment. *J. Appl. Polym. Sci.* **1995**, *57*, 969−982.
(66) Uekert, T.; Kuehnel, M. F.; Wakerley, D. W.; Reisner, E. Plastic waste as a feedstock for solar-driven H_2 generation. *Energy Environ. Sci.* **2018**, *11*, 2853−2857.
(67) Uekert, T.; Kasap, H.; Reisner, E. Photoreforming of nonrecyclable plastic waste over a carbon nitride/nickel phosphide catalyst. *J. Am. Chem. Soc.* **2019**, *141*, 15201−15210.
(68) Zhu, K. C.; Jia, H. Z.; Zhao, S.; Xia, T. J.; Guo, X. T.; Wang, T. C.; Zhu, L. Y. Formation of environmentally persistent free radicals on microplastics under light irradiation. *Environ. Sci. Technol.* **2019**, *53*, 8177−8186.
(69) Gewert, B.; Plassmann, M. M.; MacLeod, M. Pathways for degradation of plastic polymers floating in the marine environment. *Environ. Sci.: Processes Impacts* **2015**, *17*, 1513−1521.

https://doi.org/10.1021/acsestengg.1c00323
ACS EST Engg. 2022, 2, 110−120